

Data Processing Techniques for Ion and Electron Energy Distribution Functions

A. Caldarelli ^{*,1} F. Filleul ^{*,2, a)} R.W. Boswell,³ C. Charles,³ N.J. Rattenbury,² and J.E. Cater¹

¹⁾ Te Pūnaha Ātea - Auckland Space Institute, Department of Engineering Science, The University of Auckland, Auckland, 1010, New Zealand

²⁾ Te Pūnaha Ātea - Auckland Space Institute, Department of Physics, The University of Auckland, Auckland, 1010, New Zealand

³⁾ Space Plasma, Power and Propulsion Laboratory, Research School of Physics, The Australian National University, Canberra, ACT 2601, Australia

(Dated: November 8, 2022)

Retarding field energy analyzers and Langmuir probes are routinely used to obtain ion and electron energy distribution functions (IEDF, EEDF). These typically require knowledge of the first and second derivatives of the I - V characteristics, both of which can be obtained in various ways. This poses challenges inherent to differentiating noisy signals, a frequent problem with electric-probe plasma diagnostics. A brief review of commonly used analog and numerical filtering and differentiation techniques is presented, together with their application on experimental data collected in a radio-frequency plasma. The application of each method is detailed with regards to the obtained IEDF and EEDF, the deduced plasma parameters, dynamic range, energy resolution and signal distortion.

I. INTRODUCTION

Distribution functions offer a detailed description of plasma charged particles: from obtaining some useful plasma parameters (e.g. density, temperature and potential) to deducing heating and transport mechanisms, collision and reaction rates, as well as detecting the presence of particles sub-populations¹⁻⁴. The ion-energy distribution function (IEDF) is extensively employed to characterize the ion kinetics in plasma processing techniques and in the development of spacecraft electric propulsion technologies, where the detection of accelerated ion populations, such as ion beams, is important^{2,5,6}. The electron-energy distribution function (EEDF) gives an extensive picture of the dynamics of electrons. This is essential for characterizing the plasma generation mechanisms in laboratory and commercial plasma devices, as well as in investigating fundamental aspects of plasma physics, e.g. the thermodynamics of magnetized electrons^{7,8}.

Electrostatic probes, such as retarding field energy analyzers (RFEA) and single Langmuir probes (LP), are some of the most common instruments for measuring ion and electron distribution functions, respectively. The plasma potential, and the ion beam potential and density are usually obtained through the first derivative of an RFEA I - V characteristic. From a Langmuir probe I - V characteristic, the floating potential, electron temperature, plasma density, and plasma potential can be inferred via the classical Langmuir method^{9,10}. While popular thanks to its apparent simplicity, this method is only valid for plasmas with Maxwellian electron distributions and can

be inaccurate in determining the plasma potential and ion current^{11,12}. Alternatively, the Druyvesteyn method directly determines the electron distribution function from the second derivative of the LP I - V characteristics, a process inherently more robust and information-rich than the Langmuir method, yet more challenging owing to the double differentiation¹³.

The ion-energy distribution function has usually been computed by obtaining the first derivative of the collected current over the discriminator voltage^{2,5,6,14-19}. It can be shown that, by assuming a one-dimensional velocity distribution¹⁴, the ion-energy distribution $g_i(\varepsilon_i)$ is proportional to the negative derivative of the collected current I_C with respect to the discriminator grid voltage V_D :

$$g_i(\varepsilon_i) = -\frac{1}{t^4 A_o e^2} \sqrt{\frac{m_i}{2eV}} \frac{dI_C}{dV_D}, \quad (1)$$

where t is the probe grid transmission factor (four grids in the case of the RFEA used in this work)², A_o is the area of the probe orifice, and m_i is the ion mass. Thus, the IEDF can be calculated simply by differentiating the measured current with respect to the discriminator voltage. For a single Gaussian distribution, the voltage at which the IEDF peak occurs is defined as the local plasma potential, V_p . If a population of accelerating ions is present, as in the case of a plasma expanding through a double-layer^{2,18,20} and for the considered gas pressures (i.e., ~ 0.2 - 1 mTorr), the IEDF would show a second peak at a higher energy located at the ion beam potential, V_B .

Druyvesteyn¹³ showed that for an isotropic plasma, the EEDF is proportional to the second derivative of the electron current from the I - V characteristic of a Langmuir probe. The relationship between the EEDF and the second derivative of the LP electron current I_e with

* These authors contributed equally to this work

^{a)} Electronic mail: felicien.filleul@auckland.ac.nz

respect to the biasing voltage V_{bias} is

$$g_{\text{ed}}(\varepsilon_e) = \frac{2\sqrt{2m_e e V}}{A_p e^3} \frac{d^2 I_e}{dV_{\text{bias}}^2}. \quad (2)$$

Here, $V = V_p - V_{\text{bias}}$ and V_p is the local plasma potential. ε_e is the electron energy in electronvolts, A_p is the probe area, e is the elementary charge and m_e the electron mass. The electron probability distribution function (EEDF) is then $g_{\text{ep}}(\varepsilon_e) = g_{\text{ed}}(\varepsilon_e)/\sqrt{\varepsilon_e}$. In an isotropic electron gas, the EEDF and EEPF contain the same information as the electron distribution function (which includes the velocity space). The local plasma potential V_p is found from the zero crossing of $d^2 I_e / dV_{\text{bias}}^2$. The electron density can be retrieved from

$$n_e = \int_0^\infty g_{\text{ed}}(\varepsilon_e) d\varepsilon_e, \quad (3)$$

and the effective electron temperature T_{eff} can be calculated from the average electron energy $\langle \varepsilon_e \rangle$ as

$$T_{\text{eff}} = \frac{2}{3} \langle \varepsilon_e \rangle = \frac{2}{3} \int_0^\infty \varepsilon_e g_{\text{ed}}(\varepsilon_e) d\varepsilon_e. \quad (4)$$

Plotting the natural logarithm of the EEPF can show a departure from a Maxwellian energy distribution function if the slope of the EEPF is not linear, e.g. bi-Maxwellian or Druyvesteynian. If the EEPF is Maxwellian, the electron temperature can also be deduced from the slope of the natural logarithm of the EEPF and is equal to T_{eff} .

IEDF and EEDF are usually obtained through a variety of analog and numerical differentiation routines. Since measurement noise amplification is inherent to the differentiation process, filtering/fitting methods may be necessary to smooth the measured I - V data without causing significant distortion and to obtain accurate first and second derivatives. Among the numerical methods, the Savitzky-Golay filter is one of the most commonly employed for IEDF/EEDF derivations^{21–25}. Fernández Palop *et al.*²⁶ implemented a Gaussian filter to smooth the I - V characteristics and evaluate the electron-energy distribution function. This method was compared with the Savitzky-Golay filter and the B-spline approximation methods. Magnus and Gudmundsson²⁷ compared the use of the Savitzky-Golay filter, as well as the Gaussian filter, the Blackman window and polynomial fitting, to smooth both simulated and experimental I - V curves. The mean squared error, the correlation coefficient and the residuals of the different methods were compared, coupled with a visual assessment of the EEPF. Alternatively, analog differentiation has been performed by using appropriate electronics circuitry to obtain the IEDF and the EEPF^{3,17,28–30}. The IEDF has also been obtained using a Gaussian deconvolution method^{2,16,19}.

The aim of this paper is to review different signal processing and differentiation methods for the acquisition of optimal ion- and electron-energy distribution functions. The study discusses analog and numerical processing techniques that are routinely used to obtain EEDFs

and IEDFs. With respect to the latter, the focus is on processing IEDFs that show the presence of multiple ion populations. The different numerical processes reviewed to obtain the first and second derivatives from the I - V characteristics are: Savitzky-Golay (SG) filter, B-spline piecewise polynomial fitting (BS), Gaussian filter (GF), and the Blackman window filter (BW). The ion-energy distribution function is also computed using the Gaussian deconvolution method. The analysis presented is intended as a baseline approach for the manipulation of I - V characteristics obtained from experimental data in a plasma discharge. Specifically, data collected in a magnetized radio-frequency plasma discharge at low gas pressures are used, which contain a higher noise level than, e.g. DC plasma discharges. This work gathers the lessons learned in the acquisition and processing of electric probe data to ease the reader's process of obtaining charged-particles energy distribution functions of suitable quality.

The work is organized as follows; [Section II](#) describes the experimental set-up, including the plasma diagnostic probes. [Section III](#) introduces the analog and numerical filtering/differentiation methods employed. Finally, [Section IV](#) provides an example application of data processing analysis for ion- and electron-energy distribution functions obtained from the different methods starting from raw experimental data.

II. APPARATUS & DIAGNOSTICS

A. Apparatus

The data used in this study has been acquired using *Moa*³¹, a radio-frequency plasma reactor that is an expansion of *Huia*^{32,33}. It consists of a 150 cm long, 9 cm inner diameter borosilicate glass tube plasma source connected to a 70 cm long, 50 cm diameter steel expansion chamber hosting the pumping system and the pressure gauges. The location of the interface between the plasma source and the expansion chamber is defined as $(r, z) = (0, 0)$ cm. A base pressure of $\sim 10^{-7}$ Torr is routinely achieved, while the argon working pressure ranges between 0.5×10^{-3} Torr and 1×10^{-3} Torr. The plasma is triggered and energized in the plasma source using a 1-1/3 turns loop antenna connected through an L-type matching network to a 1 kW RF generator working at 27.12 MHz. A static magnetic field is applied with a pair of movable Helmholtz solenoids, placed concentrically with the glass tube. The coils position along the plasma source length can be adjusted to obtain the desired magnetic field topology.

B. Retarding Field Energy Analyzer

The retarding field energy analyzer used to measure the ion-energy distribution function consists of four mesh grids (namely, earth, repeller, discriminator, and secondary grid) and a nickel collector plate that collects the

incoming ion flux. The grids are made of a nickel mesh with a transmission factor of 59% which are attached to a copper support. The probe orifice has a diameter of 2 mm, and a 0.1 mm thick polyimide sheet is used to electrically insulate the grids and the collector plate. The design of this probe has been extensively used in similar experiments^{2,15,18,34}, and a detailed description of the RFEA and its electric circuit used herein are presented in Ref. 35. In order to map the energy of the ions, the voltage of the discriminator grid is swept from 0 V to 80 V to obtain the I - V characteristics. It has to be noted that from RFEA measurements, only the energy distribution function of the ions that fall through the probe sheath within an acceptance angle of $\pm 40^\circ$ are obtained². When taking measurements of the ion current in an RF plasma with an RFEA, the collected data can be affected by different mechanisms. In particular, in an RF excited plasma, broadening of the energy distribution caused by RF modulation can be observed^{2,15,36} that could lead to peak separation, giving false data on the presence of different ion populations. Additionally, possible ion-neutral collisions (elastic and charge-exchange) occurring in the probe sheath and inside the analyzer could also affect the collected ion energy. However, for the low-pressure case analyzed, collisions inside the RFEA and in the sheath can be considered negligible, i.e. $\lambda_i \gg s, d$ (where s is the sheath width in front of the RFEA and d is the repeller-discriminator grid distance).

C. RF Compensated Langmuir Probe

As from Langmuir's work, sizing a single Langmuir probe requires the plasma volume disturbed by the probe to be much smaller than the electron mean free path λ_e ¹¹. This ensures that the probe only disturbs the plasma in ways that can be accounted for by theory. Following recommendations in Ref. 12, Langmuir's theory is satisfied if the probe tip radius r_p , the tip length l_p , the tip holder radius r_h and the local Debye length λ_D all satisfy the condition $r_p \ln(\pi l_p / 4 r_p), r_h, \lambda_D \ll \lambda_e$. Moreover, to guarantee Druyvesteyn's isotropic plasma condition in the presence of an applied magnetic field, the probe tip should be kept perpendicular to the streamlines and the tip radius be much smaller than the electron Larmor radius¹¹. To meet these conditions, the LP used in this work is made from a tungsten tip with $r_p = 25 \mu\text{m}$ and $l_p = 3 \text{ mm}$, mounted at the extremity of a glass pipette tapering down to $r_h = 0.75 \text{ mm}$.

Measuring an EEDF requires biasing the LP above the local plasma potential and can typically draw electron currents in the order of a few milliamperes. Therefore, in order to close the LP electric path and to ensure that all the biasing voltage is developed across the probe sheath, the existence of a low impedance sheath at conductive walls should be verified (see Ref. 11 for more details). For this purpose a grounded aluminium sleeve of adequate surface area was inserted inside the dielectric plasma

source tube at the end opposite to the diffusion chamber³².

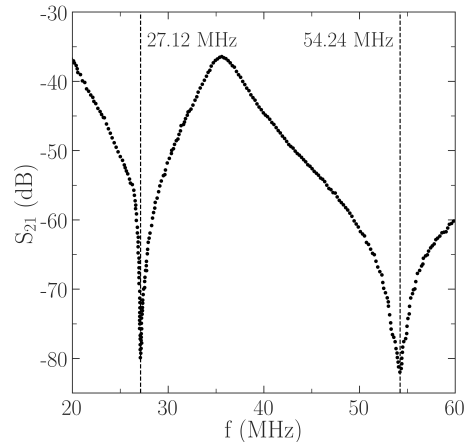


Figure 1. The attenuation spectrum of the RF compensated probe used in this study.

With the loop antenna capacitive coupling to the plasma, oscillations of the plasma potential at the applied radio-frequency and its harmonics are known to cause severe distortions to LP I - V characteristics^{11,37}. While this effect is not easily visible in the probe I - V characteristic, it becomes evident with the second derivative and, without proper mitigation, it severely compromises EEDF studies. Because the root-mean-square of V_p at the first and second harmonics are larger than $T_e/2$ in the present apparatus, RF compensation was added to the Langmuir probe, following design steps described in detail in Sudit and Chen³⁷ and Godyak and Demidov¹¹. Four resonant chokes (*TE Connectivity SC30100KT*) and a reference electrode were incorporated in the probe head. The chokes self-resonant frequencies (SFR) were tuned to 27.12 MHz and 54.24 MHz with shunt capacitors of appropriate values. The filter is housed inside the glass pipette, placed as close as possible to the probe tip to minimize stray capacitance. Shown in Fig. 1, the attenuation spectrum of the completed probe is checked with a spectrum analyzer for eventual detuning induced by the housing and adjacent wiring. The achieved attenuation of at least -80 dB at the first and second harmonics provides sufficient filter impedance to suppress the V_p RF oscillations. The reference electrode, connected to the probe tip through a capacitor, reduces the probe sheath impedance to ensure that the measuring tip follows the the plasma potential RF oscillations. For chokes containing ferrite cores, care should be taken to ensure that the ferrite does not saturate under the applied magnetic field or else the SFR will be shifted. The chokes employed were confirmed to be unaffected at the applied magnetic field strength of 300 G. The maximum probe biasing voltage was adjusted to $V_{\text{bias}} \simeq V_p + 5 \text{ V}$ to avoid excessive electron current collection which could damage the probe tip or modify its work function. Tip contamination effects were monitored by checking for hysteresis in the up and down sweeps of V_{bias} . Probe cleaning by ion bombardment was used

when necessary.

D. Data Collection

The Langmuir probe is mounted on a movable dog-legged eccentric dielectric shaft which can span the entire length of the plasma source tube³². The RFEA is mounted on a movable (rotation and translation) 6.35 mm diameter steel shaft introduced in the top port of the expansion chamber, with the probe orifice facing the plasma source exit to detect any possible directional ion beam. The LP current is deduced by measuring the voltage drop across a resistor with an isolation amplifier. The output of the amplifier is then split and fed into both a data acquisition system (DAQ) for digitization, and into an analog differentiator which outputs the first and second time derivatives. The LP V_{bias} and the RFEA V_D are defined by several periods of a triangle wave function. The data acquisition is triggered by the output on the function generator to ensure signal synchronicity and the voltages are digitized at 4,000 samples per period. One LP measurement is the average of 100 V_{bias} sweeps, while one RFEA measurement averages 200 V_D sweeps.

III. DATA PROCESSING METHODS

Obtaining an accurate IEDF or EEDF requires choosing between different techniques to compute the first and second derivative of the I - V characteristics. An ideal method would provide an undistorted derivative with a signal-to-noise ratio (S/N) equal or lower to the raw data S/N. However, in practice there is a trade-off between noise level reduction and data distortion. Fortunately, analog and numerical methods can typically combine both noise filtering and differentiation of the raw I - V data. Some of the most commonly used numerical routines are presented in this section: the Savitzky-Golay filter, the B-spline fitting, the Gaussian and the Blackman filters, together with an analog differentiation technique. The Gaussian deconvolution method to obtain IEDFs is also described.

A. Analog Differentiation

The use of analog differentiator circuits predates numerical differentiation methods, and they are still regularly employed for obtaining EEDFs and occasionally for IEDFs^{3,4,17,29,30}. The active analog differentiator used in this study, designed to work with a sweeping frequency of 10 Hz, follows the design described in Takahashi *et al.*³⁸. Two cascading operational amplifiers (*Renesas CA3140*) are each tuned to resonate at ~ 800 Hz by adjusting the resistors and capacitors values. This results in a linear gain frequency increase of 20 dB per decade up to the resonance frequency, i.e. input signals of frequencies up

to ~ 800 Hz are time-differentiated. Beyond the resonance frequency, the circuit acts as an integrator as the gain linearly decreases until becoming less than unity at ~ 80 kHz. Therefore the analog differentiator configuration also works as a band-pass filter, attenuating high frequency noise. Since real-world circuits deviate from the ideal-case, the linearity was checked to be strictly valid up to at least ~ 150 Hz. Each stage of the analog differentiator gives an output proportional to the first and second time derivative of the probe $I(t)$ signal. Knowing the biasing/discriminator voltage sweep period and voltage swing, the differentiator output can be multiplied by dt/dV to retrieve the dI_p/dV derivative. Differentiator circuits have the advantage of producing repeatable outputs since no tuning of parameters for different experimental conditions are needed. This simplifies and speeds up the data processing.

B. Polynomial Methods

A polynomial least-squares regression to model the data using a single polynomial of degree N via a least squares method has been previously attempted, giving poor results²⁷. Since the I - V characteristics of interest can be visualized as part exponential and part linear, a single polynomial regression would require a high order to fit the data to a satisfactory level, e.g. $N > 20$, with N the polynomial degree²⁷. This leads to Runge's phenomenon and over-fitting³⁹, which is visible in the results presented by Magnus and Gudmundsson²⁷. Another shortcoming is the non-locality of the polynomial fit, i.e. distant data points directly impact the local fit⁴⁰. The SG filter and the B-spline methods both circumvent these problems by fitting low degree polynomials to subsets of the data.

1. Savitzky-Golay Filter

The Savitzky-Golay filter is frequently used for smoothing and differentiating current-voltage characteristics of Langmuir probes and RFEAs^{23,25,41,42}. The filtering is achieved by doing a running fitting of a polynomial of degree N using the least-squares method on a subset of the (x, y) experimental data of width $M > N$ centered around a given point x_i (forcing M to strictly be an odd number). Evaluating the resulting polynomial at x_i gives the smoothed value Y_i and the process is repeated for x_{i+1} etc. Owing to the nature of this process, the first and last $\frac{M-1}{2}$ data points should be disregarded or the original data-set extrapolated by $\frac{M-1}{2}$ extra points at both ends.

Savitzky and Golay²¹ showed that for equally spaced data points, an analytical solution to the least-squares polynomial smoothing exists. Each one of the $N+1$ coefficients of the least-squares polynomial fitting is computed as a linear combination of the y data points inside the subset of width M . It was further demonstrated that

the coefficients of the linear combinations are function of (N, M) only. These can be tabulated for all (N, M) pairs and applying the filter only requires convolution of the coefficients with the raw data²¹. A benefit of this property is that the smoothed signal can be differentiated N times by convolution with the N^{th} derivative of the fitting polynomial, i.e. with the appropriate convolution coefficients⁴³. This avoids having to recourse to numerical finite difference methods which tend to decrease the S/N. This can be understood by considering that the differential operator in the frequency domain is proportional to the frequency itself. For a given M , the pairs $N = 0 - 1, 2 - 3, 4 - 5$, etc. give the same convolution coefficients for smoothing the raw data and evaluating the even derivatives, while $N = 1 - 2, 3 - 4, 5 - 6$ give the same coefficients for odd derivatives⁴³. Therefore for a given M , using $N = 2$ gives an identically smoothed 2nd derivative as using $N = 3$.

The SG filter acts as a low-pass filter with a flat pass-band whose cut-off frequency is a function of N and M . The cut-off frequency typically increases with N and decreases with M ⁴³. For large M , the benefit of lower cut-off frequencies is compromised by distortions of the higher frequency content of the data. On the other hand, a large N can preserve the narrow features of a signal (such as peaks) but at the cost of increasing the cut-off frequency⁴⁴. Obtaining an optimal filtering therefore requires an iterative process and a trade-off between the values of N and M .

2. B-spline Fitting

The piecewise polynomial approach used for data smoothing is the cardinal or uniform B-spline method⁴⁵. This polynomial fitting method avoids Runge's phenomenon by making use of a piecewise approach: the data is split in $k + 1$ pieces joined by k equidistant points called knots. Like other polynomial regressions, the fitting polynomial $f(x)$, or spline function, of degree N can be expressed as a linear combination of coefficients β_i and $k + N + 1$ basis functions (polynomials) $B_{i,N}(x)$:

$$f(x) = \sum_i \beta_i B_{i,N}(x). \quad (5)$$

Spline functions can therefore be calculated on different bases and the B-spline is a particular case for basis functions with local support, i.e. taking non-zero values only inside the interval on which they are defined, which spans $N + 2$ knots. As a result, this method results in a higher numerical stability compared to other splines⁴⁰. The spline function f is fitted to the data by using the least-square principle to calculate the $k + N + 1$ coefficients β_i . Additionally, the continuity conditions need to be verified, such that the function is $N - 1$ times differentiable at the knots and that $f'' = f''' = 0$ at the endpoints. The larger the number of knots, the higher the accuracy of the data fitting. However, more knots may result in over-fitting

and/or poor noise rejection. A small number of knots could also over-smooth the data. As for the SG filter, the first and second derivatives of f can be analytically derived.

C. Window Filters

1. Gaussian Filter

The Gaussian filter was developed by Hayden⁴⁶ who introduced a new smoothing routine involving the use of a Gaussian distribution function as a filter. Fernández Palop *et al.*²⁶ and Magnus and Gudmundsson²⁷ used this algorithm to smooth the I - V characteristics measured with a Langmuir probe and obtain the electron-energy probability function. The working principle of the Gaussian filter is based on the assumption that the response function of the instrument and its electronics can be approximated as a Gaussian distribution with a given standard deviation σ :

$$g(x) = \frac{1}{\sigma\sqrt{2\pi}} \exp\left\{-\frac{x^2}{2\sigma^2}\right\}. \quad (6)$$

The measured signal can then be calculated from the convolution of the experimental data d with g ($d * g$). Because the noise is not correlated with the instrument response function, g can be used for noise suppression. Owing to the property $(d * g)' = d' * g = d * g'$, the raw data can be convolved with the first and second derivative of the Gaussian function in order to obtain the first and second derivative of the I - V characteristic instead of using the central difference method. Nevertheless, for the sake of comparison with earlier results²⁷, the central difference method was used to evaluate the derivatives.

2. Blackman Window Filter

The Blackman window w is a standard moving average window, having zero value outside a chosen interval. It has been previously used to filter I - V characteristics in EEPF applications by Magnus and Gudmundsson²⁷ and Roh *et al.*⁴⁷. The Blackman window is defined by only one filtering parameter, i.e. the window size M :

$$w(n) = 0.42 - 0.5 \cos\left(\frac{2\pi n}{M}\right) + 0.08 \cos\left(\frac{4\pi n}{M}\right), \quad (7)$$

$$0 \leq n \leq M.$$

It is characterised by the highest reduction in the sidelobe level (down to ≈ -58 dB) when compared to the other window functions (e.g. Hanning)⁴⁸. However, it has a wider mainlobe resulting in a less sharp transition band in the passband of the filter that can be improved by choosing a wider window size. The derivatives cannot be obtained analytically for the Blackman window, thus a central difference operator was used after filtering the raw I - V data.

D. Gaussian Deconvolution

The Gaussian deconvolution method, or Gaussian fitting, has been used to obtain the ion-energy distribution function from the I - V characteristics measured by a retarding field energy analyzer^{2,16,19}. This involves an iterative process of integrating a Gaussian curve that models the ion-energy distribution function until the raw I - V data are reconstructed. The fitting can either be manual, or an automatic Gaussian fitting algorithm can be implemented that minimises the sum of the squared errors between the measured and the reconstructed data.

For a single ion population, the ion-energy distribution function can be modeled with a Gaussian curve

$$g(V_D) = ae^{-\left(\frac{V_D - V_{\text{peak}}}{c}\right)^2}, \quad (8)$$

where the parameters to be fit are: the amplitude a , the curve width c , and the location of the Gaussian peak V_{peak} . When a second ion population is present, as in the case of an accelerated ion beam in a collisional plasma, the IEDF requires the fitting of two or three Gaussian curves which are summed to accurately model the measured I - V curve^{2,18}. An advantage of this technique is that it does not involve any filtering or differentiation steps since the IEDF is obtained in a retrograde approach.

IV. EXAMPLE OF APPLICATION ON A DATA SET

A. Optimization of Numerical Methods

The optimal evaluation of the ion and/or energy distribution functions through numerical methods requires a compromise in the choice of parameters to achieve sufficient noise-reduction without causing significant distortion of the fitted I - V characteristics that could lead to large errors in the inferred plasma parameters and loss of information.

An analysis similar to that used by Fernández Palop *et al.*²⁶ and Magnus and Gudmundsson²⁷ is used to assess the numerical methods in this work. It is noted that in Ref. 26 and Ref. 27, the comparison of the different techniques was conducted on simulated I - V characteristics, while in this study only experimental data are used. The following parameters, evaluated between the raw probe collected current I_p and the processed data I_f , were considered: the mean squared error (MSE) and the Shapiro-Wilk (SW) test statistic W .

When comparing different regression models, an optimal processing technique would return the lowest mean squared error. However, because the MSE value can range between zero and any larger number depending on the scale of the variables, it does not provide a standardized metric to assess how well the processing actually models the observed data. Moreover, the MSE on its own does not provide a way to highlight under-smoothing and over-fitting as these situations could return the lowest

possible MSE. Thus, an analysis of the distribution of the residuals ($I_p - I_f$) is necessary to complement the MSE. In particular, verifying that the residuals are normally distributed ensures that the data processing does not significantly distort the I - V features⁴⁹. The Shapiro-Wilk test checks the null-hypothesis that the residuals are normally distributed by comparing the computed statistic $0 < W < 1$ with tabulated values^{50,51}. For a given significance level, if W is smaller than the tabulated value then the null-hypothesis can be rejected, i.e. the residuals are not normally distributed. Since filtering and fitting always somewhat distorts the data, one should aim to maximize W and re-evaluate the data processing when the null-hypothesis is rejected. Taking a 0.01 significance level and given the samples size used in this study, the null-hypothesis is rejected if $W < 0.996$ ⁵¹. Therefore, a parametric analysis is conducted together with a visual optimization of the IEDF and EEPF for determining the optimal parameters for each numerical method. The assessment requires a trade-off between minimizing the MSE, maximizing W and minimizing alterations of the raw I - V characteristic features.

Table I. Mean-squared error and Shapiro-Wilk test for different values of degree N and number of knots k of the B-spline applied to the RFEA data in Fig. 2.

N	k	MSE/ 10^{-4} (μA^2)	W
3	5	45.62	0.9935
3	15	9.25	0.9989
3	35	8.92	0.9985
3	80	8.87	0.9985
2	15	9.42	0.9987
4	15	9.75	0.9986

Specifically, the optimization of the IEDFs involves the careful computation of the first and second peak of the energy distributions, while achieving enough noise reduction when evaluating dI_C/dV_D . An excessive smoothing of the I - V characteristics would modify the voltage at which the I - V curves present the gradient changes that corresponds to the center of two ion populations present. In turn, this would yield an incorrect evaluation of the plasma and ion beam potentials, and an inaccurate derivation of the ion-energy distribution. The dependency of the choice of the numerical processing parameters on the quality of the ion-energy distribution function was studied for each numerical method. Figure 2 shows an example of the effect of the parameter choices on the first derivative for different values of polynomial degree N and number of knots k using the B-spline technique. The mean-squared error and the Shapiro-Wilk test are evaluated for each case, and the values are reported in Table I. When analyzing the dependence of the fitted polynomial degree N while $k = 15$ is kept constant, the MSE is seen to increase with N , W to decrease and the floor ripple level to increase (the Runge phenomenon). Since the I_f obtained from a B-spline of degree N is $N - 1$ continuously

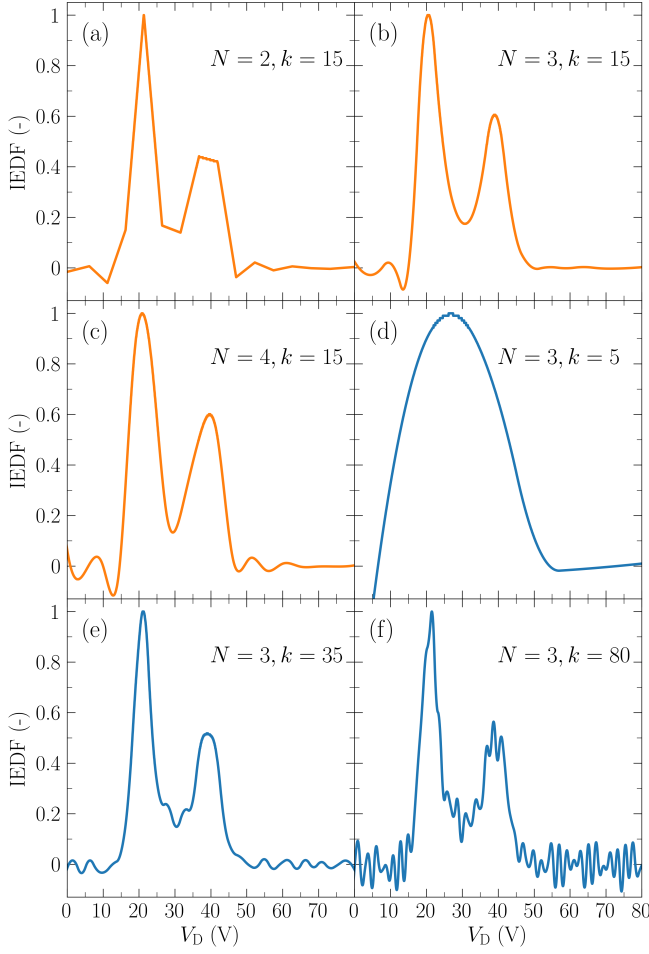


Figure 2. Normalized first derivative of the I - V characteristics measured by the RFEA obtained with the B-Spline polynomial for various values of degree N (a)-(c), and number of knots k (d)-(f).

differentiable, a quadratic B-spline does not provide a smooth first derivative (see Fig. 2 (a)). By extension, $N = 4$ is the lowest B-spline degree that can be used to obtain a smooth second derivative for the EEPF. If the number of knots is too small the evaluated IEDF is over-smoothed and the features of the I - V characteristic are distorted ($W < 0.996$ for $N = 3$ and $k = 5$). In contrast, as shown in Fig. 2 (f), too high a number of knots causes an insufficient smoothing of the noise, which could make it difficult to determine the location of the peaks. For the data analyzed in this study, a degree of $N = 3$ and a number of knots $k = 15$ are chosen for the B-spline polynomial since they result in the optimal IEDF i.e., lowest curve distortion and sufficient noise reduction.

Similarly, optimal evaluation of the EEDFs requires simultaneously maximizing the energy resolution and the dynamic range (DR). The energy resolution is characterized by the low-energy depletion δ_{ε_e} which is defined as the ε_e value of the maximum of the EEDF. Because the bulk of the electrons are in the low-energy region of the EEPF, the larger δ_{ε_e} , the larger the errors in determining n_e and

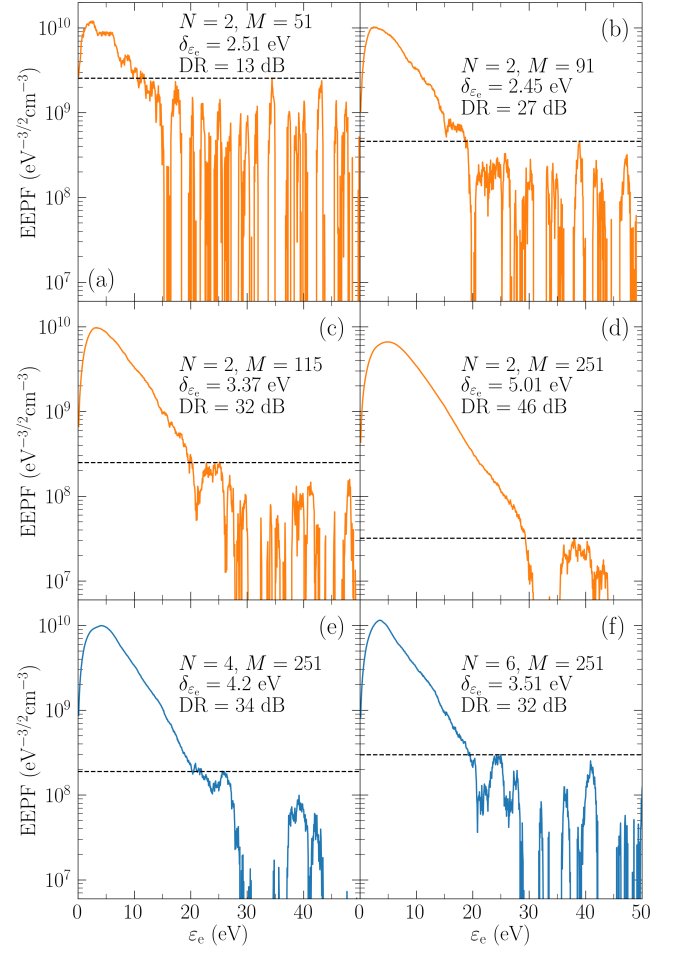


Figure 3. EEPFs obtained from applying the Savitzky-Golay filter on an LP I - V curve for $N = 2$ and increasing window size M (a)-(d) and $M = 251$ with increasing value of N (e)-(f). The horizontal dashed lines mark the minimum resolvable values of the EEPFs.

Table II. Mean-squared error (MSE) and Shapiro-Wilk test (W) for various values of degree N and window size M of the Savitzky-Golay applied to the LP data shown in Fig. 3.

N	M	MSE/ 10^{-4} (mA ²)	W
2	51	8.17	0.9973
2	91	8.50	0.9961
2	115	9.08	0.9964
2	251	4.37	0.7135
4	251	1.16	0.9132
6	251	8.86	0.9937

T_{eff} from Eq. 3 and Eq. 4. An EEDF is considered to have sufficient energy resolution if $\delta_{\varepsilon_e} \leq (0.3 - 0.5)T_e$ ^{11,12}. The dynamic range of the EEPF is defined as the ratio of its maximum to its minimum resolvable value. A dynamic range ≥ 60 dB (equivalently of 3 orders of magnitude and above) is necessary to resolve high-energy electrons in the inelastic range of the EEPF, which are detrimen-

tal in investigating excitation, ionization, and transport processes^{11,12}. An EEDF is often separated into its elastic and inelastic ranges, defined as $\varepsilon_e < \varepsilon_e^*$ and $\varepsilon_e > \varepsilon_e^*$, respectively. ε_e^* is the lowest excitation energy of the working gas, e.g. 11.55 eV for argon⁵². Minimizing δ_{ε_e} and maximizing the DR is therefore paramount in the process of determining the optimal numerical parameters, together with minimizing the MSE and maximizing the value of W .

Figure 3 shows an example of the impact of varying the polynomial degree N and moving window size M of the Savitzky-Golay filter when applied to a compensated LP I - V characteristic acquired with the experimental apparatus. For each (N, M) pair, the corresponding MSE and Shapiro-Wilk test statistic W are given in Table II. In Fig. 3 (a)-(d) $N = 2$, and the effect of increasing M is shown. As expected for an SG filter, increasing M is beneficial from the dynamic range point-of-view since it improves from 13 dB to 46 dB owing to the decreasing cut-off frequency. However, this is accompanied by distortions of the signal, visible from the worsening of the low-energy resolution δ_{ε_e} , the MSE and W . Fixing M and increasing N to the next even integers (since $N = 2$ and $N = 3$ produce the same output), the signal distortion improves again at the cost of decreasing the DR, as shown in Fig. 3 (d)-(f) and Table II. Regarding the Shapiro-Wilk test, all the cases with $M = 251$ failed the normality test with $W < 0.996$. Overall, trading-off between δ_{ε_e} , the DR, the MSE and W , the best performing filter for this data is for $(N = 2, M = 115)$. It is noted that none of the (N, M) pairs produced an EEPF fulfilling the aforementioned requirements, since the dynamic range never reaches 3 orders of magnitude. Different (N, M) pairs can be used whether the goal of obtaining the EEPF lies in the study of elastic or inelastic processes. Alternatively, the outputs of two SG filter applications could be combined into a high resolution and high dynamic range numerically derived EEPF, with the drawback of a more complicated post-processing⁴⁷.

B. Ion-Energy Distribution Function (IEDF)

As mentioned in Section I, the ion-energy distribution function can be derived from the first derivative of the measurements acquired with a retarding field energy analyzer. The respective I - V characteristics was taken in the expansion chamber with the RFEA orifice located 19 cm downstream of the magnetic nozzle ($z_p = 19$ cm). The experimental conditions were maintained at an RF power of 250 W, argon pressure in the chamber of 0.5 mTorr, and a maximum magnetic field on axis of $B_{z,\max} = 330$ G. Under these conditions, the plasma density peaks axially under the solenoids reaching a value of $\approx 10^{12} \text{ cm}^{-3}$ which then decreases to $\sim 10^{10} \text{ cm}^{-3}$ in the expansion chamber. The data processing of the collected current $I_C(V_D)$ measured with the energy analyzer and the subsequent computation of the ion-energy distribution function

followed the approach described in Section IV A.

Table IV summarizes the results of the parametric analysis that provide the smoothest IEDF possible for the numerical smoothing methods analyzed, while keeping intact the peak features. Figure 4 shows the ion-energy distribution functions obtained with the different analog and numerical techniques from experimental data. The IEDFs plotted are normalized by their peak value, and the position of the two peaks, i.e. the local plasma potential and the ion beam potential, is also reported. The data in Fig. 4 has a signal-to-noise ratio of approximately 66 dB. The raw I - V curve, shown in Fig. 4 (a), was obtained by averaging 200 consecutive probe sweeps and it is plotted with the fitted Gaussian deconvolution to illustrate one of the data processing methods. As seen in Fig. 4, the ion-energy distribution functions show a double-peak feature indicating the presence of a bi-population of ions: the first peak represents the background ion population (at zero energy) which location can be considered the local plasma potential V_p , while the second peak corresponds to the accelerated ion beam population with potential V_B end energy $\varepsilon_B = e(V_B - V_p)$. Comparing measurements taken with a source-facing and a radial-facing RFEA shows that the IEDF does not present a peak separation effect due to RF modulation, but it effectively detects the presence of a directional ion beam³¹. It is also noted that the ion-neutral mean free path for the operating pressure of 0.5 mTorr is shorter than the distance between the source exit and the probe position i.e., $\lambda_i \sim 10$ cm and $z_p = 19$ cm. Thus, the accelerated ion beam component is decreased at the measurement location while the local, background ion population is enhanced due to charge-exchange collisions. Furthermore, elastic collisions could affect the beam direction, further reducing the collected beam current.

Table III presents the key results obtained with the different data processing techniques, namely: the local plasma potential V_p , the ion beam potential V_B , the mean squared error (MSE), and the Shapiro-Wilk test statistic W . The Gaussian deconvolution method required the fitting of three Gaussian curves to accurately model the two ion populations.

Table III. Results of the different IEDF processing methods in Fig. 4 (a).

Method	V_p (V)	V_B (V)	MSE/ 10^{-4} (μA^2)	W
Analog	21.03	39.02	-	-
Gaussian deconv.	20.94	39.07	9.16	0.9990
SG	20.90	39.07	8.97	0.9986
B-spline	20.58	39.03	9.25	0.9989
GF	21.16	38.61	9.08	0.9984
BW	21.16	38.61	9.15	0.9984

Comparing the analog differentiation method and the numerical techniques, it is evident that both the plasma and ion beam potentials are approximately unchanged with a standard deviations for V_p and V_B of ± 0.21 V

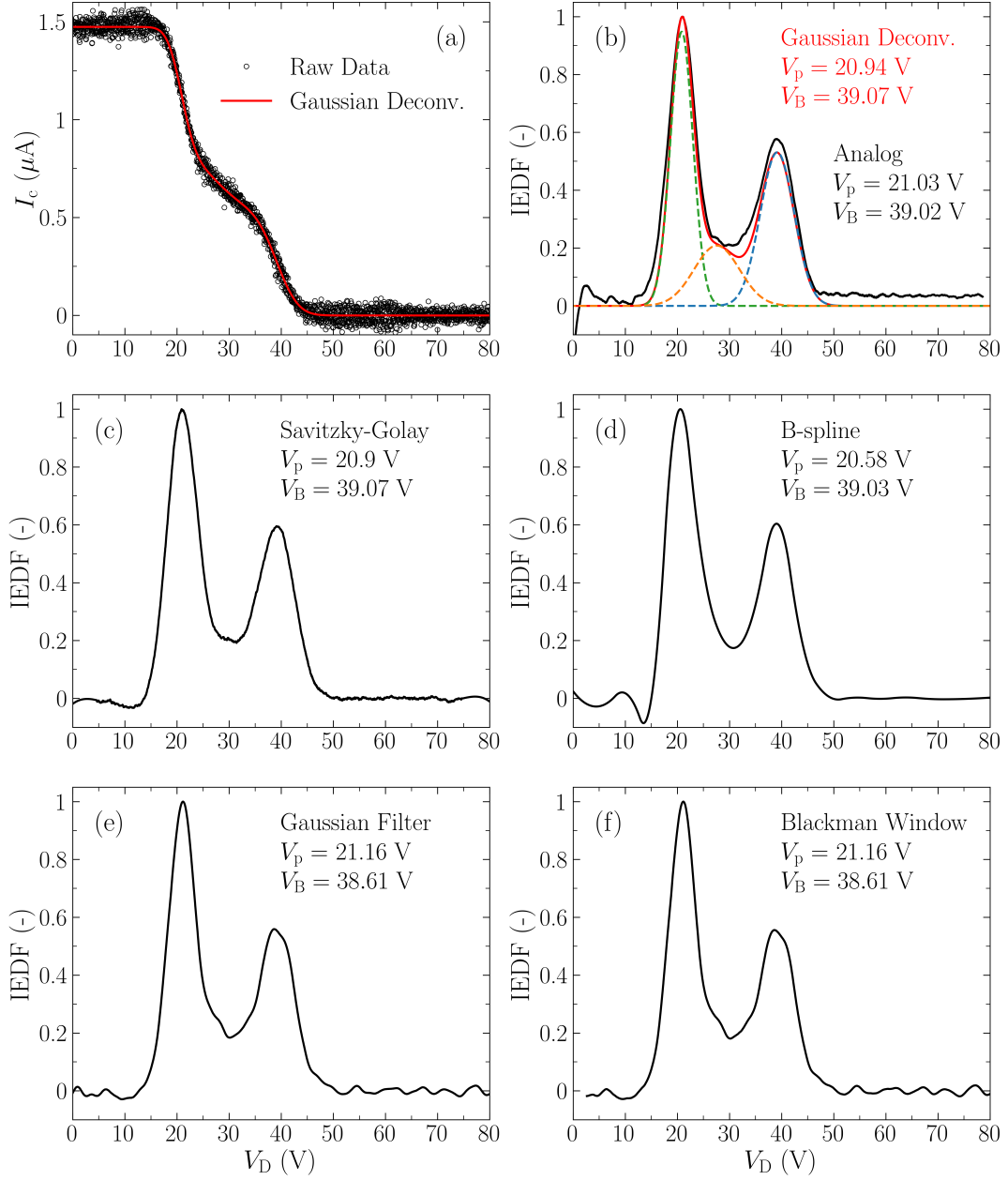


Figure 4. Results of the analog and numerical differentiation and filtering methods from RFEA measurements showing the raw I - V characteristics with the integrated Gaussian deconvolution curve (a), and the ion-energy distribution functions against the discriminator voltage obtained with: the analog differentiator (black line) and the Gaussian deconvolution method (red line) (b), the Savitzky-Golay filter (c), The B-spline polynomial (d), the Gaussian filter (e), and the Blackman Window filter (f). The dashed curves in (b) represent the three fitted curves resulting from the Gaussian deconvolution method.

and ± 0.23 V, respectively. For the collected data, all the smoothing methods perform well in terms of mean squared error and the SW test statistic. The MSEs are $\leq 9.25 \times 10^{-4} \mu\text{A}^2$ for all techniques, while the calculated W values are all higher than 0.998. The Savitzky-Golay filter yields the lowest MSE, while the Gaussian deconvolution methods performs the best in the SW test, resulting in the highest W . It has to be noted that the Blackman filter showed an overshoot of the fitted polynomial at the edges caused by the zero padding in the convolution; this was

addressed by disregarding the initial data points as the plasma characteristics in that region were not of interest.

C. Electron-Energy Probability Function (EPPF)

The RF compensated LP data were acquired with the apparatus operated at 200 W of RF power, 1 mTorr of argon, $B_{z,\text{max}} = 300$ G and with the Helmholtz solenoids placed 30 cm away from the loop antenna. These condi-

Table IV. Set of parameters for the processing used of the I - V characteristics in Fig. 4 and Fig. 5.

Method	Differentiation	Window size M		Degree N		Sigma σ		Knots k	
		EEPF	IEDF	EEPF	IEDF	EEPF	IEDF	EEPF	IEDF
Savitzky-Golay Filter	Analytic	115	301	2	4	-	-	-	-
B-spline Fitting	Analytic	-	-	5	3	-	-	42	15
Gaussian Filter	Analytic	-	-	-	-	25	24	-	-
Blackman Window	Central Difference	156	140	-	-	-	-	-	-

tions create an inductively coupled plasma exhibiting a symmetrical single peaked axial plasma density gradient ranging from 10^{12} cm^{-3} under the solenoids to 10^{10} cm^{-3} at the extremities of the glass tube^{32,33,53}. The LP was placed on axis halfway between the antenna and the solenoids. The processing of $I_p(V_{\text{bias}})$ to obtain the EEPF with the analog and numerical methods was conducted following the steps described in Section IV A. Table IV gives the resulting optimal numerical parameters.

Figure 5 (a) shows the raw I - V LP characteristic together with the optimized Savitzky-Golay filter output from Fig. 3, i.e. for $(N = 2, M = 115)$. As reference, the signal-to-noise ratio of the LP characteristic is 48 dB. In Fig. 5 (b)-(f), the EEPFs obtained from the various methods and the deduced plasma parameters are shown. T_{eff} and n_e are calculated by integrating the EEPF according to Eq. 4 and Eq. 3, respectively. Their values are reported together with V_p , the MSE, W , dynamic range and energy resolution for each method in Table V. The maximum variance in the obtained values of V_p is less than 2%. Likewise, for T_{eff} and n_e , their maximum variances are $\sim 13\%$ and $\sim 8\%$, respectively. Thus, in terms of estimating the plasma parameters, all 5 methods have comparable performance, i.e. within the absolute error tolerances usually associated with LP measurements^{4,12}.

In terms of energy resolution and dynamic range, different methods perform best depending on whether the focus is on resolving low-energy or high-energy electrons dynamics and properties. The B-spline fitting in Fig. 5 (d) resulted in the best energy resolution at $\delta_{\varepsilon_e} \simeq 2.3 \text{ eV}$ and is the only method to satisfy the $\delta_{\varepsilon_e} \leq (0.3 - 0.5)T_e$ condition. The second-best performing method is the analog differentiation with $\delta_{\varepsilon_e} \simeq 3.2 \text{ eV}$, i.e. 0.375 eV away from satisfying the energy resolution condition. Regardless of the employed method, the energy resolution is ultimately limited by the absence of internal resistance compensation in the present LP implementation, in particular of the plasma-wall sheath impedance, or by the probe tip surface condition¹². Techniques to further improve the resolution are available in Ref. 12 and 47.

The analog differentiation method in Fig. 5 (b) resulted in an EEPF with a significantly larger dynamic range of approximately 3 orders of magnitude, compared to 2 orders of magnitude for the numerical methods. The analog differentiation is therefore the only method presented which can reliably resolve inelastic processes and can provide confidence on the nature of the electron distribution function, i.e. a single-Maxwellian for ε_e up to 30 eV in the

present case. This is further highlighted in Fig. 5 (b) by the linear regression of the EEPF, shown by a dashed red line. The same linear regression applied to the numerically derived EEPFs highlights that the reduced DR and artificial oscillations in the case of the B-spline would make it difficult to reach conclusions on the nature of the electron distribution function. Among the numerical methods, the Savitzky-Golay and the B-spline are the best performing for this data set, with the lowest distortion of the original I - V curve, as shown by their lower mean-square errors and Shapiro-Wilk test statistics in Table V. The Gaussian and Blackman window filters both resulted in noticeable distortions of the data ($W < 0.996$, i.e. their residuals are not normally distributed), in particular around the plasma floating potential and plasma potential portions of the I - V curve.

Finally, it is interesting to note that following the guidelines in Ref. 12, the low-energy gap δ_{ε_e} impacts can be corrected by extrapolating the EEPF from its linear portion down to $\varepsilon_e = 0 \text{ eV}$ when the right conditions are satisfied. Because electron-electron collisions are the dominant processes for thermalizing electrons and making the distribution Maxwellian, and since the frequency of these collisions is inversely proportional to $\varepsilon_e^{3/2}$, if the EEPF is Maxwellian for some ε_e greater than the energy of EEPF peak, then the EEPF is likely to be Maxwellian at lower energies^{12,54,55}. This extrapolation can be achieved with the linear regressions shown in Fig. 5 as dashed red curves. Applying this process to the analog EEPF in Fig. 5 (b) for example, the effective electron temperature obtained with the corrected EEPF is $T_{\text{eff}}' = 4.32 \text{ eV}$ and the corrected electron density $n_{e'} = 2.57 \times 10^{11} \text{ cm}^{-3}$, to compare with the values in Table V. The electron temperature obtained from the slope of the linear regression is $T_{e,\text{fit}} = 4.2 \text{ eV}$, providing evidence that the low-energy extrapolation has closely recovered the original EEPF shape.

V. CONCLUSIONS

This review outlines some of the most frequently employed data processing methods to obtain ion and electron-energy distribution functions from I - V characteristics measured with a retarding field energy analyzer and an RF compensated Langmuir probe, respectively. Design recommendations relevant to measurements in RF magnetized plasmas are presented for both instruments. After

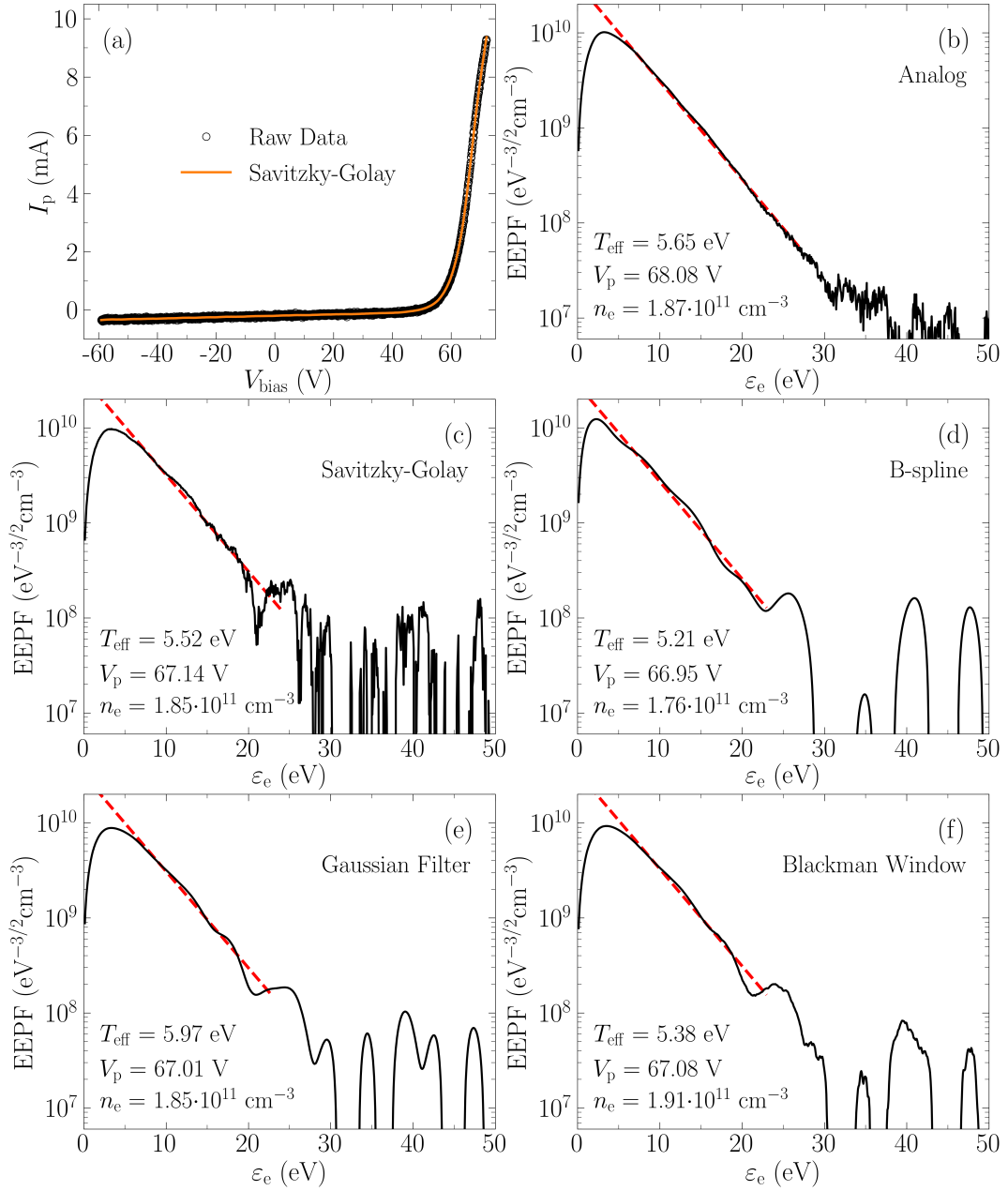


Figure 5. Comparison of the analog and numerical methods for obtaining the EEPF, showing the raw I - V characteristics (a), the EEPF obtained from the analog differentiator (b) and from the different numerical methods (c)-(f). The red dashed lines are the linear fit used to extract the electron temperature $T_{e,\text{fit}}$.

Table V. Results of the different EEPF processing methods in Fig. 5.

Method	V_p (V)	T_{eff} (eV)	$n_e/10^{11}$ (cm^{-3})	MSE/ 10^{-3} (mA^2)	W	DR (dB)	δ_{ϵ_e} (eV)
Analog	68.08	5.65	1.87	-	-	55	3.2
SG	67.14	5.52	1.85	0.91	0.9964	32	3.4
B-spline	66.95	5.21	1.76	0.84	0.997	36	2.3
GF	67.01	5.97	1.85	3.3	0.8015	33	3.4
BW	67.08	5.38	1.91	3.1	0.8537	33	3.5

describing the different processing techniques, an example of a parametric analysis to obtain optimal IEDFs and

EEPFs is presented and applied to experimental data sets collected in a magnetized RF plasma apparatus. The

recommended parameters optimization involves checking the mean-squared error and the normal distribution of the residuals (i.e. the Shapiro-Wilk test), coupled with a visual assessment process to ensure sufficient noise reduction with minimal distortion of the curves.

With respect to the IEDF, the analysis focused on the evaluation of first derivatives that accurately represented a plasma containing a bi-population of ions. For the data set under study, both the analog and numerical methods provide smooth IEDFs and consistent values of the local plasma and the ion beam potentials. Regarding the numerical methods analyzed, they all perform well in terms of MSE and W ; in particular, the Savitzky-Golay filter and the Gaussian deconvolution methods delivered the best results in terms of obtaining accurate IEDFs with the least data distortion.

The EEPFs obtained from each method are assessed in terms of maximizing the energy resolution and dynamic range while minimizing distortions of the Langmuir probe I - V curve. Among the numerical methods, the Savitzky-Golay filter and the B-spline fitting performed best in terms of distortion and energy resolution. All numerical methods delivered a mediocre dynamic range of approximately 2 orders of magnitude, which is to be related to the experimental data set employed having a low signal-to-noise ratio of 48 dB. This could make it challenging to confidently identify the nature of the electron distribution function and to study inelastic electron processes. This is in contrast with the EEPF obtained from the same I - V curve using the analog differentiator which showed a dynamic range of approximately 3 orders of magnitude and can be clearly identified as being Maxwellian up to ~ 30 eV. When the intent of calculating the EEPF is solely to obtain the plasma parameters, all methods explored are found to deliver equivalent results. The analog differentiator technique provides an appreciable reduction in the IEDF and EEPF processing time compared to the numerical methods since no data-set specific optimization is required.

DATA AVAILABILITY STATEMENT

The data that support the findings of this study are available from the corresponding author upon reasonable request.

AUTHOR CONTRIBUTIONS

In alphabetical order, A.C. and F.F. share first authorship. A.C. and F.F. performed the data acquisition, data processing and manuscript preparation concerning the IEDF and EEDF, respectively. R.B. and C.C. provided guidance in experimental RF plasmas and diagnostics. N.R. and J.C. are doctoral supervisors of A.C. and F.F.

CONFLICT OF INTEREST STATEMENT

The authors declare that the research was conducted in the absence of any commercial or financial relationships that could be construed as a potential conflict of interest.

REFERENCES

- V. Godyak, R. Piejak, and B. Alexandrovich, "Probe diagnostics of non-Maxwellian plasmas," *Journal of Applied Physics* **73**, 3657–3663 (1993).
- C. Charles and R. Boswell, "Laboratory evidence of a supersonic ion beam generated by a current-free "helicon" double-layer," *Physics of Plasmas* **11**, 1706–1714 (2004).
- K. Takahashi, C. Charles, R. Boswell, W. Cox, and R. Hatakeyama, "Transport of energetic electrons in a magnetically expanding helicon double layer plasma," *Applied Physics Letters* **94**, 191503 (2009).
- R. W. Boswell, K. Takahashi, C. Charles, and I. D. Kaganovich, "Non-local electron energy probability function in a plasma expanding along a magnetic nozzle," *Frontiers in Physics* **3**, 14 (2015).
- S. Ingram and N. S. J. Braithwaite, "Ion and electron energy analysis at a surface in an RF discharge," *Journal of Physics D: Applied Physics* **21**, 1496 (1988).
- L. Hahl, D. Rafalskyi, and T. Lafleur, "Ion beam diagnostic for the assessment of miniaturized electric propulsion systems," *Review of Scientific Instruments* **91**, 093501 (2020).
- V. Godyak, R. Piejak, and B. Alexandrovich, "Evolution of the electron-energy-distribution function during rf discharge transition to the high-voltage mode," *Physical Review Letters* **68**, 40 (1992).
- K. Takahashi, C. Charles, R. W. Boswell, and A. Ando, "Thermodynamic analogy for electrons interacting with a magnetic nozzle," *Physical Review Letters* **125**, 165001 (2020).
- H. M. Mott-Smith and I. Langmuir, "The theory of collectors in gaseous discharges," *Physical Review* **28**, 727 (1926).
- R. L. Merlino, "Understanding Langmuir probe current-voltage characteristics," *American Journal of Physics* **75**, 1078–1085 (2007).
- V. Godyak and V. Demidov, "Probe measurements of electron-energy distributions in plasmas: what can we measure and how can we achieve reliable results?" *Journal of Physics D: Applied Physics* **44**, 233001 (2011).
- V. Godyak, "RF discharge diagnostics: Some problems and their resolution," *Journal of Applied Physics* **129**, 041101 (2021).
- M. J. Druyvesteyn, "Der niedervoltbogen," *Zeitschrift für Physik* **64**, 781–798 (1930).
- C. Böhm and J. Perrin, "Retarding-field analyzer for measurements of ion energy distributions and secondary electron emission coefficients in low-pressure radio frequency discharges," *Review of Scientific Instruments* **64**, 31–44 (1993).
- C. Charles, A. W. Degeling, T. E. Sheridan, J. H. Harris, M. A. Lieberman, and R. W. Boswell, "Absolute measurements and modeling of radio frequency electric fields using a retarding field energy analyzer," *Physics of Plasmas* **7**, 5232–5241 (2000).
- W. Cox, C. Charles, R. W. Boswell, and R. Hawkins, "Spatial retarding field energy analyzer measurements downstream of a helicon double layer plasma," *Applied Physics Letters* **93**, 071505 (2008).
- K. Takahashi, Y. Shida, and T. Fujiwara, "Magnetic-field-induced enhancement of ion beam energy in a magnetically expanding plasma using permanent magnets," *Plasma Sources Science and Technology* **19**, 025004 (2010).
- A. Bennet, C. Charles, and R. Boswell, "In situ electrostatic characterisation of ion beams in the region of ion acceleration," *Physics of Plasmas* **25**, 023516 (2018).

- ¹⁹R. Imai and K. Takahashi, "Deflections of dynamic momentum flux and electron diamagnetic thrust in a magnetically steered rf plasma thruster," *Journal of Physics D: Applied Physics* **55**, 135201 (2022).
- ²⁰A. M. Keesee, E. E. Scime, C. Charles, A. Meige, and R. Boswell, "The ion velocity distribution function in a current-free double layer," *Physics of Plasmas* **12**, 093502 (2005).
- ²¹A. Savitzky and M. J. E. Golay, "Smoothing and Differentiation of Data by Simplified Least Squares Procedures," *Analytical Chemistry* **36**, 1627–1639 (1964).
- ²²I. D. Sudit and R. C. Woods, "A workstation based Langmuir probe system for low-pressure dc plasmas," *Review of Scientific Instruments* **64**, 2440–2448 (1993).
- ²³S. Bétchu, A. Soum-Glaude, A. Bès, A. Lacoste, P. Svarnas, S. Aleiferis, A. Ivanov Jr, and M. Bacal, "Multi-dipolar microwave plasmas and their application to negative ion production," *Physics of Plasmas* **20**, 101601 (2013).
- ²⁴L. Conde, J. L. Domenech-Garret, J. M. Donoso, J. Damba, S. P. Tierno, E. Alamillo-Gamboa, and M. A. Castillo, "Supersonic plasma beams with controlled speed generated by the alternative low power hybrid ion engine (ALPHIE) for space propulsion," *Physics of Plasmas* **24**, 123514 (2017).
- ²⁵J. Damba, P. Argente, P. Maldonado, A. Cervone, J.-L. Domenech-Garret, and L. Conde, "Multiprobe characterization of plasma flows for space propulsion," *Journal of Physics: Conference Series* **958**, 012002 (2018).
- ²⁶J. Fernández Palop, J. Ballesteros, V. Colomer, and M. Hernández, "A new smoothing method for obtaining the electron energy distribution function in plasmas by the numerical differentiation of the I-V probe characteristic," *Review of Scientific Instruments* **66**, 4625–4636 (1995).
- ²⁷F. Magnus and J. T. Gudmundsson, "Digital smoothing of the Langmuir probe I-V characteristic," *Review of Scientific Instruments* **79**, 073503 (2008).
- ²⁸R. Sloane and E. MacGregor, "An alternating current method for collector analysis of discharge-tubes," *The London, Edinburgh, and Dublin Philosophical Magazine and Journal of Science* **18**, 193–207 (1934).
- ²⁹V. Godyak, R. Piejak, and B. Alexandrovich, "Measurement of electron energy distribution in low-pressure rf discharges," *Plasma Sources Science and Technology* **1**, 36 (1992).
- ³⁰S. Yadav, S. Ghosh, S. Bose, K. Barada, R. Pal, and P. Chattopadhyay, "Role of ion magnetization in formation of radial density profile in magnetically expanding plasma produced by helicon antenna," *Physics of Plasmas* **25**, 043518 (2018).
- ³¹A. Caldarelli, F. Filleul, C. Charles, R. Boswell, N. Rattenbury, and J. Cater, "Radial characterization of an ion beam in a deflected magnetic nozzle," *Journal of Electric Propulsion* **1**, 10 (2022).
- ³²F. Filleul, A. Caldarelli, C. Charles, R. Boswell, N. Rattenbury, and J. Cater, "Characterization of a new variable magnetic field linear plasma device," *Physics of Plasmas* **28**, 123514 (2021).
- ³³F. Filleul, A. Caldarelli, R. Boswell, C. Charles, N. Rattenbury, and J. Cater, "The role of ion magnetization on plasma generation in a magnetic nozzle rf device," *Journal of Electric Propulsion* **1**, 20 (2022).
- ³⁴W. Cox, C. Charles, R. W. Boswell, R. Laine, and M. Perren, "Magnetic ion beam deflection in the helicon double-layer thruster," *Journal of Propulsion and Power* **26**, 1045–1052 (2010).
- ³⁵A. Caldarelli, F. Filleul, C. Charles, N. Rattenbury, and J. Cater, "Preliminary Measurements of a Magnetic Steering System for RF Plasma Thruster Applications," in *AIAA Propulsion and Energy 2021 Forum* (2021) p. 3401.
- ³⁶G. D. Conway, A. J. Perry, and R. W. Boswell, "Evolution of ion and electron energy distributions in pulsed helicon plasma discharges," *Plasma Sources Science and Technology* **7**, 337–347 (1998).
- ³⁷I. D. Sudit and F. F. Chen, "RF compensated probes for high-density discharges," *Plasma Sources Science and Technology* **3**, 162 (1994).
- ³⁸K. Takahashi, C. Charles, R. Boswell, M. A. Lieberman, and R. Hatakeyama, "Characterization of the temperature of free electrons diffusing from a magnetically expanding current-free double layer plasma," *Journal of Physics D: Applied Physics* **43**, 162001 (2010).
- ³⁹G. Celant and M. Broniatowski, *Interpolation and Extrapolation Optimal Designs 1: Polynomial Regression and Approximation Theory* (John Wiley & Sons, New York, 2016, pp. 57–62).
- ⁴⁰A. Perperoglou, W. Sauerbrei, M. Abrahamowicz, and M. Schmid, "A review of spline function procedures in R," *BMC Medical Research Methodology* **19**, 1–16 (2019).
- ⁴¹K. G. Xu and M. L. Walker, "Plume Characterization of an Ion-Focusing Hall Thruster," *Journal of Propulsion and Power* **28**, 1105–1115 (2012).
- ⁴²N. Gulbrandsen and Å. Fredriksen, "RFEA Measurements of High-Energy Electrons in a Helicon Plasma Device with Expanding Magnetic Field," *Frontiers in Physics* **5** (2017), 10.3389/fphy.2017.00002.
- ⁴³J. Luo, K. Ying, P. He, and J. Bai, "Properties of Savitzky-Golay digital differentiators," *Digital Signal Processing* **15**, 122–136 (2005).
- ⁴⁴W. H. Press and S. A. Teukolsky, "Savitzky-Golay Smoothing Filters," *Computers in Physics* **4**, 669–672 (1990).
- ⁴⁵C. De Boor and C. De Boor, *A practical guide to splines*, Vol. 27 (Springer-Verlag New York, 2001).
- ⁴⁶H. C. Hayden, "Data smoothing routine," *Computers in Physics* **1**, 74–75 (1987).
- ⁴⁷H.-J. Roh, N.-K. Kim, S. Ryu, S. Park, S.-H. Lee, S.-R. Huh, and G.-H. Kim, "Determination of electron energy probability function in low-temperature plasmas from current - Voltage characteristics of two Langmuir probes filtered by Savitzky-Golay and Blackman window methods," *Current Applied Physics* **15**, 1173–1183 (2015).
- ⁴⁸R. Chassaing, *Digital signal processing and applications with the C6713 and C6416 DSK* (Wiley-Interscience, Hoboken, N.J., 2005).
- ⁴⁹A. K. Sen and A. Sen, *Regression analysis : theory, methods and applications* (Springer-Verlag, New York, 1990).
- ⁵⁰S. S. Shapiro and M. B. Wilk, "An analysis of variance test for normality (complete samples)," *Biometrika* **52**, 591–611 (1965).
- ⁵¹M. M. Rahman and Z. Govindarajulu, "A modification of the test of shapiro and wilk for normality," *Journal of Applied Statistics* **24**, 219–236 (1997).
- ⁵²V. Puech and L. Torchin, "Collision cross sections and electron swarm parameters in argon," *Journal of Physics D: Applied Physics* **19**, 2309 (1986).
- ⁵³A. Bennet, C. Charles, and R. Boswell, "Non-local plasma generation in a magnetic nozzle," *Physics of Plasmas* **26**, 072107 (2019).
- ⁵⁴L. Tsendin, "Electron kinetics in glows—from Langmuir to the present," *Plasma Sources Science and Technology* **18**, 014020 (2009).
- ⁵⁵I. Kaganovich, V. Demidov, S. Adams, and Y. Raites, "Non-local collisionless and collisional electron transport in low-temperature plasma," *Plasma Physics and Controlled Fusion* **51**, 124003 (2009).